

Physics-Informed Neural Nets-based Control

Eric Aislan Antonelo^a, Eduardo Camponogara^a, Laio Oriel Seman^a, Eduardo Rehbein de Souza^a, Jean P. Jordanou^a, Jomi F. Hübner^a

^a*Department of Automation and Systems Engineering, Federal University of Santa Catarina, Florianópolis - Brazil*

Abstract

Physics-informed neural networks (PINNs) impose known physical laws into the learning of deep neural networks, making sure they respect the physics of the process while decreasing the demand of labeled data. For systems represented by Ordinary Differential Equations (ODEs), the conventional PINN has a continuous time input variable and outputs the solution of the corresponding ODE. In their original form, PINNs do not allow control inputs neither can they simulate for long-range intervals without serious degradation in their predictions. In this context, this work presents a new framework called *Physics-Informed Neural Nets-based Control* (PINC), which proposes a novel PINN-based architecture that is amenable to control problems and able to simulate for longer-range time horizons that are not fixed beforehand. First, the network is augmented with new inputs to account for the initial state of the system and the control action. Then, the response over the complete time horizon is split such that each smaller interval constitutes a solution of the ODE conditioned on the fixed values of initial state and control action. The complete response is formed by setting the initial state of the next interval to the terminal state of the previous one. The new methodology enables the optimal control of dynamic systems, making feasible to integrate a priori knowledge from experts and data collected from plants in control applications. We showcase our method in the control of two nonlinear dynamic systems: the Van der Pol oscillator and the four-tank system.

Keywords: physics-informed neural networks, nonlinear model predictive control, deep learning.

1. Introduction

The competition in today's globalized world is a driving force for the digitalization of enterprises, an initiative known as industry 4.0, which is making increasingly necessary the simulation and control of complex real-world systems in smart and efficient ways. To face the challenges in this context, harnessing deep learning for smart automation and control of real plants is not only desirable but also inevitable.

The power of deep learning comes from its data-driven nature to solve complex problems. When we view the learning problem as a minimization of a

cost function that can be augmented according to particular criteria, beneficial properties can be embedded into the deep network’s learning. For instance, the learning problem’s cost function can be augmented to include additional terms that help regularize the learning itself. Regularization is usually achieved by Ridge Regression [1] for least-squares problems or by weight decay in neural networks (or ℓ_2 -norm regularization) [2], although several other methods are also available [3]. Both of them add penalties on the ℓ_2 -norms of the network weights, avoiding high magnitudes for the weight parameters while improving the trained network’s generalization property.

While those regularization methods have proved to be very useful in machine learning, an alternative way to regularize supervised learning tasks consists of using the underlying process’s known physical laws. As such, a deep neural network can learn the required behavior not only from data, but also from a priori knowledge built previously by experts or borrowed from the laws of nature. This research area has been expanding quickly, mainly under the denomination of Physics-Informed Neural Networks (PINN) [4, 5].

A standard PINN has a continuous-time t as input, and the system’s state variables as output \mathbf{y} . The main outcome of this approach is that the need for real data collection is reduced to a minimum, since the behavior of the deep network is constrained to follow physical laws given in terms of Partial Differential Equations (PDE) or Ordinary Differential Equations (ODE). These differential equations are included in the learning problem’s cost function as nonlinear differential operators on the outputs \mathbf{y} of the networks, defining a second cost term that regularizes the learning process. Effectively, this approach also allows solving complex PDEs or ODEs by using deep learning, since the network output \mathbf{y} represents the solution of these equations [4].

Since [4], many extensions and alternative approaches have been proposed. In [6], approximate models restricted by physical laws are presented for stochastic PDEs with high-dimensional and spatially variable coefficients. For that, they employ convolutional networks in addition to fully connected networks. In [7], PDEs of high dimensionality (up to 200 dimensions) are solved by a deep neural network trained with stochastic gradient descent and mini-batches of input points, to satisfy the differential operator, initial and boundary conditions. This is also achieved in [8]. In [9], parallel PINNs are proposed to decompose a long-term problem in several short-time independent problems. To achieve that, several smaller PINNs are trained in parallel such that each one solves the problem for a particular time interval. Approaches that embed physical constraints in unsupervised learning and reinforcement learning are found in [10]. Other recent works in the area are [11, 12].

However, to the best of our knowledge there are no PINN architectures in the literature that allow optimal control techniques such as Multiple Shooting (MS) [13] and Model-based Predictive Control [14] (MPC) to be easily applied. MPC is a technique that has become standard for multivariate control in industry and academia [15]. Since its establishment in the 1970s, MPC has been successfully applied in the oil and gas [16], aerospace [17] and process industries, as well as in robotics [18]. The main idea of MPC is to control a system by employing a

prediction model: at every iteration of the control loop, an optimization problem is solved using a model of the plant in a receding horizon approach. Previous works used neural networks such as Echo State Networks and Long Short-Term Memory networks as models of the plant or process to be controlled [19]. These networks are trained exclusively on data collected from the process and are thus not sample efficient as PINNs, as the latter can benefit from prior knowledge of the physics laws involved in the processes. In this sense, the challenge is to make PINNs compliant to control applications so that they can be used as a predictive model of a plant or a process. In their original form, PINNs do not allow control inputs, neither can they simulate for variable long-range intervals without serious degradation in their predictions.

With those limitations in mind, this work presents a new framework called *Physics-Informed Neural Nets-based Control* (PINC), which proposes a novel PINN-based architecture that is amenable to control problems. In particular:

- (i) our PINN-based architecture, called hereafter PINC net, is augmented with extra inputs such as the initial state of the system and control input, in addition to the continuous-time t . This augmentation is inspired by the multiple shooting and collocation methods [13], which are numerical methods for solving boundary value problems in ODEs, which split the time horizon over which a solution is sought into several smaller intervals (shooting intervals). In our new proposal, a single network learns the ODE solution conditioned on the initial state and the given control input over the smaller shooting interval.
- (ii) this innovation allows solving the long-range time interval problems inherent to conventional PINNs, which consists of a degradation of the network's response for large input of the time t . This is related to the maximum value allowed for t , which is fixed at training time. On the other hand, our proposed PINC network can run for an indefinite time horizon as long as it is necessary, without significant deterioration of network prediction. This is achieved by chaining the network prediction in a self-feedback mode, by setting the initial state (input) of the next interval k to the last predicted state (network output) of the previous interval $k - 1$. The work in [9] also intends to solve this problem, but it requires many individual PINNs to be independently trained and [9] is also not ready for control applications.
- (iii) finally, the particular structure of PINC makes physics-informed nets amenable to MPC applications, which is the first work in the literature to tackle this as far as the authors know.

In the context of identification and control, the PINC approach makes it feasible control applications that need to integrate both of the following: some expert knowledge known about the plant in the form of physical laws and sparse noisy data collected from the plant. Effectively, when data are costly to obtain and a physics-based model is available and known to capture the required behaviors, a surrogate model can be learned by adding a penalty term to the loss

function for imposing the a priori structure given by the physical laws. This addition strongly and informatively regularizes the surrogate model, diminishing the demand for process data. This seamless integration effected in the loss function takes the best of both worlds for improved surrogate modeling. In the following, PINNs, MPC and PINC are presented in Section 2, whereas the experiments on identifying and controlling two known dynamical systems in the literature are shown in Section 3. Section 4 concludes this work.

2. Methods

2.1. Physics-informed Neural Networks (PINNs)

In [4, 5], physics-informed neural networks are introduced, whereby deep neural networks are trained in a supervised way to respect any physical law described by partial differential equations (PDEs). The PINN approach allows one to find data-driven solutions of PDEs or ODEs automatically. In this paper, nonlinear ODEs are considered of the following general form:

$$\partial_t \mathbf{y} + \mathcal{N}[\mathbf{y}] = 0, \quad t \in [0, T] \quad (1)$$

where $\mathcal{N}[\cdot]$ is a nonlinear differential operator and \mathbf{y} represents the state of the dynamic system (the latent ODE solution).

We define $\mathcal{F}(\mathbf{y})$ to be equivalent to the left-hand side of Equation (1):

$$\mathcal{F}(\mathbf{y}) := \partial_t \mathbf{y} + \mathcal{N}[\mathbf{y}] \quad (2)$$

Here, \mathbf{y} also represents the output of a multilayer neural network (hence the notation \mathbf{y} instead of \mathbf{x}) which has the continuous time t as input: $\mathbf{y} = f_{\mathbf{w}}(t)$, where $f_{\mathbf{w}}$ represents the mapping function obtained by a deep network parametrized by adaptive weights \mathbf{w} . This formulation implies that a neural network must learn to compute the solution of a given ODE.

Assuming an autonomous system for this formulation, a given neural network $\mathbf{y}(t)$ is trained using optimizers such as Adam [20] or L-FGBS [21] to minimize a mean squared error (MSE) cost function:

$$\text{MSE} = \text{MSE}_y + \text{MSE}_{\mathcal{F}}, \quad (3)$$

where

$$\text{MSE}_y = \frac{1}{N_y} \sum_{i=1}^{N_y} \frac{1}{N_t} \sum_{j=1}^{N_t} |y_i(t^j) - \hat{y}_i^j|^2, \quad (4a)$$

$$\text{MSE}_{\mathcal{F}} = \frac{1}{N_y} \sum_{i=1}^{N_y} \frac{1}{N_{\mathcal{F}}} \sum_{k=1}^{N_{\mathcal{F}}} |\mathcal{F}(y_i(t^k))|^2, \quad (4b)$$

where: N_t , $N_{\mathcal{F}}$, and N_y correspond to the number of training data samples, the number of collocation points, and the number of outputs of the neural

network, respectively; $y_i(\cdot)$ is the i -th output of the network; \hat{y}_i^j represents the desired i -th output for $y_i(\cdot)$, considering the j -th data pair (t^j, \hat{y}_i^j) . The first loss term MSE_y corresponds to the usual cost function for regression [2] based on collected training data $\{(t^j, \hat{y}_i^j)\}_{j=1}^{N_t}$, which usually provides the boundary (initial or terminal) conditions of ODEs when solving these equations.

The second loss term $\text{MSE}_{\mathcal{F}}$ penalizes the misadjusted behavior of $\mathbf{y}(t)$, measured by $\mathcal{F}(\mathbf{y})$ in Equation (2), whereby the physical structure of the solution is imposed by $\mathcal{F}(\mathbf{y})$ at a finite set of randomly sampled collocation points $\{t^k\}_{k=1}^{N_{\mathcal{F}}}$. Experiments show that the training data size N_t required for learning a certain dynamical behavior is drastically reduced due to the a priori information assimilated from $\text{MSE}_{\mathcal{F}}$. As the differential equation of the physical system is assumed to be represented by $\mathcal{F}(\mathbf{y}) = 0$, the term $\text{MSE}_{\mathcal{F}}$ is a measure of how well the PINN adheres to the solution of the physical model. This physics-informed approach provides a framework that unifies a previously available theoretical, possibly approximate model and measured data from processes, which is capable of correcting imprecisions in the theoretical model or providing sample efficiency in process modeling.

2.2. Nonlinear Model Predictive Control

Model Predictive Control (MPC) has evolved considerably over the last two decades, achieving a significant impact on industrial process control. This impact can be attributed to its generality in posing the process control problem in the time domain, being suitable for SISO (Single Input Single Output), and MIMO (Multiple Inputs Multiple Outputs) systems. Soft and hard constraints can be imposed on the formulation of the control law through optimization problems, while minimizing an objective function over a prediction horizon [22].

MPC is not a specific control strategy, but rather a denomination of a vast set of control methods developed considering some standard ideas and predictions [22]. Figure 1 shows a representation of the output prediction at a time instant, where the proposed actions generate a predicted behavior that reduces the distance between the value predicted by the model and a reference trajectory.

The MPC strategy uses a discrete mathematical model based on the real process of interest. A predicted output is calculated in a prediction horizon by comparing the mathematical model to the real process's output. To propose control actions, the MPC strategy uses an iterative optimization process, taking into account the mathematical model of interest and the constraints that it is subjected. Based on objectives and constraints, the optimization problem is composed of mathematical expressions established in the controller's design phase, taking many forms. Usually, quadratic functions are used to penalize the error in the reference tracking.

According to [23], there are several ways to classify these controllers taking into account characteristics such as model linearity, treatment of uncertainties, and how the optimization problem is solved. In this work, we focus on the lack of model linearity, more specifically in the Nonlinear Model Predictive Control

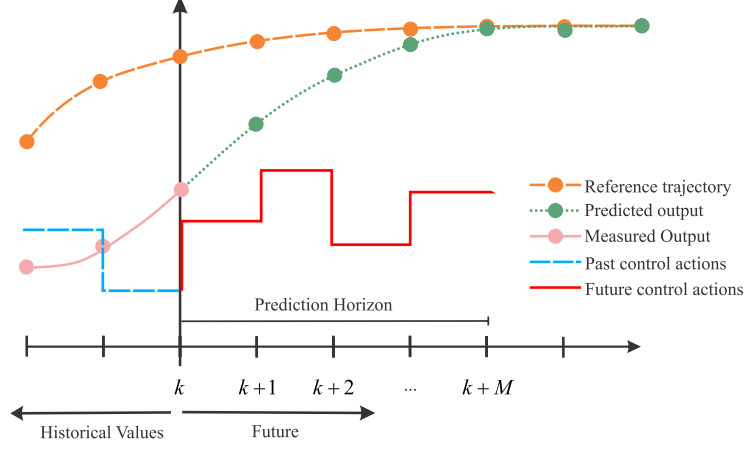


Figure 1: Representation of the output prediction in a time instant, where the proposed actions generate a predicted behavior that reduces the distance between the value predicted by the model and a reference trajectory.

(NMPC) [14]. The discrete NMPC formulation is given by:

$$J = \sum_{j=N_1}^{N_2} \left\| \mathbf{x}[k+j] - \mathbf{x}^{\text{ref}}[k+j] \right\|_{\mathbf{Q}}^2 + \sum_{i=0}^{N_u-1} \left\| \Delta \mathbf{u}[k+i] \right\|_{\mathbf{R}}^2 \quad (5a)$$

while being subject to:

$$\mathbf{x}[k+j+1] = \mathbf{f}(\mathbf{x}[k+j], \mathbf{u}[k+j]), \quad \forall j = 0, \dots, N_2 - 1 \quad (5b)$$

$$\mathbf{u}[k+j] = \mathbf{u}[k-1] + \sum_{i=0}^j \Delta \mathbf{u}[k+i], \quad \forall j = 0, \dots, (N_u - 1) \quad (5c)$$

$$\mathbf{u}[k+j] = \mathbf{u}[k+N_u-1], \quad \forall j = N_u, \dots, N_2 - 1 \quad (5d)$$

$$\mathbf{h}(\mathbf{x}[k+j], \mathbf{u}[k+j]) \leq 0, \quad \forall j = N_1, \dots, N_2 \quad (5e)$$

$$\mathbf{g}(\mathbf{x}[k+j], \mathbf{u}[k+j]) = 0, \quad \forall j = N_1, \dots, N_2 \quad (5f)$$

where k represents the time step at which the MPC problem is being computed, $\mathbf{x}[k]$ is the recurrent state of the dynamic system which, for simplification purposes, is also the output (i.e., $\mathbf{x} = \mathbf{y}$), \mathbf{x}^{ref} is the set-point signal over the prediction horizon (i.e., reference), being defined by the first penalized instant $k+N_1$ and the last instant $k+N_2$. The cost function J is the penalization of the quadratic error between the model output \mathbf{x} and the reference along the horizon \mathbf{x}^{ref} , and the penalization of the control increment $\Delta \mathbf{u}$. Each penalization is weighted by the diagonal matrices \mathbf{Q} and \mathbf{R} , respectively. Eqn. (5b) is the constraint imposed by the considered state-equation model with \mathbf{x} as the state, and equations (5e) and (5f) refer to inequality and equality constraints imposed by functions \mathbf{h} and \mathbf{g} , respectively. Eqns. (5c) and (5d) define the relation between the control action \mathbf{u} and the control increments, which are aggregated

into the control action from time k up until either the control action time $k + j$ or $k + N_u - 1$.

The optimization problem is defined by equations from (5a) to (5f) and results in a Non-Linear Programming (NLP) Problem, which can be solved using well-established methods like Sequential Quadratic Programming (SQP) [24] and the Interior-Point (IP) method, available in commercial [25] and non-commercial solvers [26]. The NLP is solved at each time step k , and typical approaches [15] only apply the first control increment into the system.

2.3. Physics-Informed Neural nets-based Control (PINC)

Unlike PINNs that assume fixed inputs and conditions, the proposed PINC framework operates with variable initial conditions as well as control inputs that can change over the complete simulation, making it suitable for model predictive control tasks. The network is augmented with two, possibly multidimensional inputs: control action \mathbf{u} and initial state $\mathbf{y}(0)$, as illustrated in Figure 2. The output of the network is given by:

$$\mathbf{y}(t) = f_{\mathbf{w}}(t, \mathbf{y}(0), \mathbf{u}), \quad t \in [0, T] \quad (6)$$

where $f_{\mathbf{w}}$ represents the mapping given by a deep network parametrized by weights \mathbf{w} . In this work, we assume the control input to be a constant value for the time interval $t \in [0, T]$. Thus, the new formulation provides a conditioned response $\mathbf{y}(t)$ on \mathbf{u} and $\mathbf{y}(0)$ during this interval of T seconds.

Traditional PINNs tend to degrade rapidly for long time intervals and can only accept input t in the range the network was trained. The PINC framework significantly alleviates this degrading issue as well as enables control applications by dividing the problem in M equidistant control time intervals, each of T seconds (see Fig. 4). We call this shorter period of T seconds as the *inner continuous time interval* of the problem, in which a solution of an ODE is obtained given some initial condition $\mathbf{y}(0)$ (which models the current system state) and control input \mathbf{u} for $t \in [0, T]$. This ODE solution $\mathbf{y}(t)$, which is the output of the network, is found by a single PINC network, that is, the same network solves all M intermediate problems, which results from learning the ODE solution for a particular range of initial conditions and control inputs that vary over the complete time horizon, but which stay constant for $t \in [0, T]$.

2.3.1. Combining the intermediate solutions

Each of the M intermediate solutions of T seconds can be viewed in Figure 4. The states $\mathbf{y}[k]$ inferred by the network can be seen at the top of the figure as a dashed trajectory, while its corresponding inputs are located in the lower part. Here, the notation changed to represent the output in discrete time k . Between steps k and $k + 1$, one intermediate solution is given by Equation (6), fixing the control input to some constant and the initial state to the last state of step $k - 1$.

Since t is an input to the network, the state at $t = T$ can be directly inferred by a single forward network propagation:

$$\mathbf{y}[k] = f_{\mathbf{w}}(T, \mathbf{y}[k-1], \mathbf{u}[k]) \quad (7)$$

where the initial state is set to the last state of the previous step, i.e., $\mathbf{y}[k-1]$; and the control input $\mathbf{u}[k]$ has an index k indicating which fixed value is applied in the inner continuous time interval between steps $k-1$ and k .

2.3.2. Free-run simulation in the prediction horizon

The initial state of the dynamical system in step k can be either the true state $\hat{\mathbf{y}}[k-1]$ coming from the process or the previous network prediction $\mathbf{y}[k-1]$ at timestep $k-1$.

Within one iteration of MPC, the PINC net is used for a certain prediction horizon without feedback from the process. This means that the network prediction $\mathbf{y}[k-1]$ and not the true state $\hat{\mathbf{y}}[k-1]$ is fed back as input to the same network in the next timestep k of the prediction horizon (Fig. 3a).

In discrete time control applications, a sampling period T_s must be chosen. The setting of T_s usually depends on the particular dynamics of the process being modeled. Here, T is equal to the sampling period T_s . Thus, using equation (7), we can encapsulate the PINC prediction function so that it is only a function of the control action $\mathbf{u}[k]$ and previous prediction $\mathbf{y}[k-1]$, leaving T implicit:

$$\begin{aligned} \mathbf{y}[k] &= \hat{f}_{\mathbf{w}}(\mathbf{y}[k-1], \mathbf{u}[k]) \\ &= f_{\mathbf{w}}(T, \mathbf{y}[k-1], \mathbf{u}[k]) \end{aligned} \quad (8)$$

We call $\hat{f}_{\mathbf{w}}$ the control interface for the PINC framework. Thus, $\frac{\partial \hat{f}_{\mathbf{w}}}{\partial \mathbf{u}}$ can be computed for providing the Jacobian matrix to solvers used in MPC, possibly by means of automatic differentiation. This control interface provides the prediction of the states of the dynamic system at the vertical lines in Fig. 4, that is, at every T_s seconds, the state $\mathbf{y}[k]$ is predicted in a single forward net propagation operation, for $k = 1, \dots, M$. This differs from numerical integration methods that need to integrate over the continuous inner interval [27].

Since the prediction is fed back as an input at every discrete timestep, it is expected that errors accumulate in the long free run. This is not exclusive of this approach, and is common to recurrent neural networks. However, because MPC works in a receding horizon control approach, at every timestep k of the control loop, the input $\mathbf{y}[k-1]$ representing the initial state is set to the real system's state $\hat{\mathbf{y}}[k-1]$ (Fig. 3b). Thus, the prediction horizon in MPC always starts from the true initial state $\hat{\mathbf{y}}[k-1]$, that is, Equation (8) becomes

$$\mathbf{y}[k] = \hat{f}_{\mathbf{w}}(\hat{\mathbf{y}}[k-1], \mathbf{u}[k]) \quad (9)$$

which counters error accumulation between consecutive control iterations.

The error might accumulate when the MPC model is used in a future finite prediction horizon to solve a constrained optimization problem. In this case, the prediction $\mathbf{y}[k-1]$ is fed back as no readings from the real process at a future time are possible (Fig. 3a).

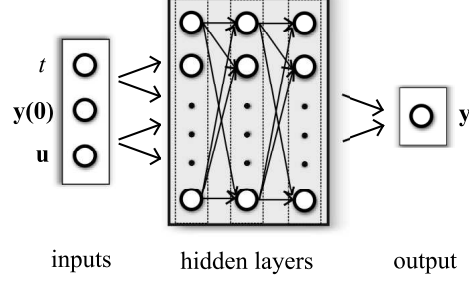


Figure 2: The PINC network has initial state $\mathbf{y}(0)$ of the dynamic system and control input \mathbf{u} as inputs, in addition to continuous time scalar t . Both $\mathbf{y}(0)$ and \mathbf{u} can be multidimensional. The output $\mathbf{y}(t)$ corresponds to the state of the dynamic system as a function of $t \in [0, T]$, and initial conditions given by $\mathbf{y}(0)$ and \mathbf{u} . The deep network is fully connected even though not all connections are shown.

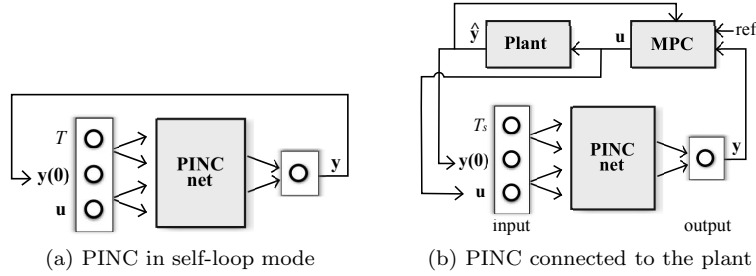


Figure 3: Modes of operation of the PINC network. (a) PINC net operates in self-loop mode, using its own output prediction as next initial state, after T seconds. This operation mode is used within one iteration of MPC, for trajectory generation until the prediction horizon of MPC completes (predicted output from Fig. 1). (b) Block diagram for PINC connected to the plant. One pass through the diagram arrows corresponds to one MPC iteration applying a control input \mathbf{u} for T_s timesteps for both plant and PINC network. Note that the initial state of the PINC net is set to the real output of the plant. In practice, in MPC, these two operation modes are executed in an alternated way (optimization in the prediction horizon, and application of control action).

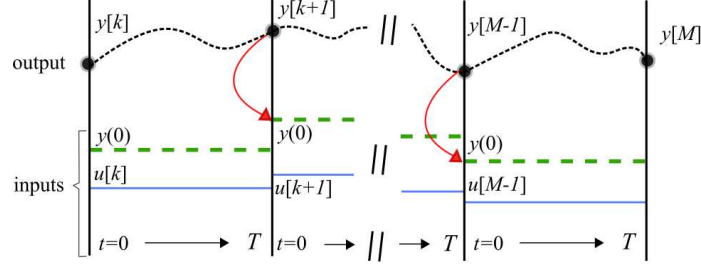


Figure 4: Representation of a trained PINC network evolving through time in self-loop mode (Fig. 3a) for trajectory generation in prediction horizon. The top dashed black curve corresponds to a predicted trajectory \mathbf{y} of a hypothetical dynamic system in continuous time. The states $\mathbf{y}[k]$ are snapshots of the system in discrete time k positioned at the equidistant vertical lines. Between two vertical lines (during the *inner continuous interval* between steps k and $k+1$), the PINC net learns the solution of an ODE with $t \in [0, T]$, conditioned on a fixed control input $\mathbf{u}[k]$ (blue solid line) and initial state $\mathbf{y}(0)$ (green thick dashed line). Control action $\mathbf{u}[k]$ is changed at the vertical lines and kept fixed for T seconds, and the initial state $\mathbf{y}(0)$ in the interval between steps k and $k+1$ is updated to the last state of the previous interval $k-1$ (indicated by the red curved arrow). The PINC net can directly predict the states at the vertical lines without the need to infer intermediate states $t < T$ as numerical simulation does. Here, we assume that $T = T_s$ and, thus, the number of discrete timesteps M is equal to the length of the prediction horizon in MPC.

2.3.3. Training

The first loss term in Equation (3) can be generalized to the PINC network as:

$$\text{MSE}_y = \frac{1}{N_y} \sum_{i=1}^{N_y} \frac{1}{N_t} \sum_{j=1}^{N_t} |y_i(\mathbf{v}^j) - \hat{y}_i^j|^2, \quad (10)$$

where the pair $(\mathbf{v}^j, \hat{\mathbf{y}}^j)$ corresponds to the j -th training example and $\mathbf{v}^j = (t, \mathbf{y}(0), \mathbf{u})^j$ is the whole input to the network (i.e., time variable, system initial state, and control input). Usually, this dataset comes from measured data, but in this work we will show that, if we assume that the given ODE is an exact representation of the process, it is enough for this dataset to contain only the initial conditions of the modelled ODE. For instance, one such training data pair is $((0, 0.4, 0.6), 0.4)$, which means: at $t = 0$ the initial state is 0.4, the control input is 0.6 and the desired output is equal to the initial state (0.4). Thus, for all data points, $t = 0$, while $\mathbf{y}(0)$ and \mathbf{u} are randomly sampled from intervals defined according to the modelled dynamic system. This means that MSE_y represents the mean squared error for all randomly sampled initial conditions of the considered ODE and control inputs. Note also that the input $\mathbf{y}^j(0)$ is equal to the desired output $\hat{\mathbf{y}}^j$ in the training set, such that the network must learn to *reproduce* the initial state $\mathbf{y}^j(0)$ into the network output $\mathbf{y}(\mathbf{v}^j)$ at $t = 0$. In practice, the aforementioned assumption allows training using randomly sampled data for solving the ODE, without ever requiring measured process's data.

The second loss term in Equation (3) is rewritten as:

$$\text{MSE}_{\mathcal{F}} = \frac{1}{N_y} \sum_{i=1}^{N_y} \frac{1}{N_{\mathcal{F}}} \sum_{k=1}^{N_{\mathcal{F}}} |\mathcal{F}(y_i(\mathbf{v}^k))|^2, \quad (11)$$

where \mathbf{v}^k corresponds to the k -th collocation point $(t, \mathbf{y}(0), \mathbf{u})^k$, where now all three types of inputs (and not only the last two), i.e., time, initial condition, and control input, are randomly sampled from their respective particular intervals. Specifically, the interval for t is $[0, T]$, where T is the *inner continuous interval* of the PINC framework.

Basically, this formulation means that the PINC net is trained with *data* points that lie on the boundary of simulations, i.e., only initial states of ODEs are presented for the loss function in (10). Practically, this does not require collecting data from ODE simulators. On the other hand, the collocation points in $\text{MSE}_{\mathcal{F}}$ serve to regularize the PINC net to satisfy the behavior defined by \mathcal{F} . Thus, in the training process, the PINC net is only directly informed with a initial state in (10), and its physics-informed cost loss in (11) must enforce the structure of the differential equation into its output $\mathbf{y}(\cdot)$ for the remaining *inner continuous interval* of T seconds (e.g., $t \in (0, T]$).

The total loss can be generalized to $\text{MSE} = \text{MSE}_y + \lambda \cdot \text{MSE}_{\mathcal{F}}$, where λ represents a rescaling factor so that both terms are approximately in the same scale. Given that the PINC net structure, datasets and the losses are defined, the training process starts with the ADAM optimizer [20] for K_1 epochs, and subsequently continues with the L-FGBS optimizer [21] for K_2 iterations in order to adapt the net weights \mathbf{w} towards the minimization of MSE. Note that automatic differentiation is employed for the physics-informed term $\text{MSE}_{\mathcal{F}}$ in (11), using deep learning frameworks such as *Tensorflow*.

2.3.4. NMPC

After training, the PINC net is used as a model in nonlinear MPC, whose algorithm is described in Section 2.2. Thus, the control interface function $\hat{f}_{\mathbf{w}}$ in Equation (8) replaces Equation (5b) in the MPC formulation, redefining the notation of a dynamic system's state by the prediction given by the PINC network, i.e., $\mathbf{x}[k] = \mathbf{y}[k]$. After these substitutions, we arrive at a Multiple Shooting (MS)-inspired formulation for the NMPC problem under the PINC framework:

$$J = \sum_{j=N_1}^{N_2} \|\mathbf{y}[k+j] - \mathbf{y}^{\text{ref}}[k+j]\|_{\mathbf{Q}}^2 + \sum_{i=0}^{N_u-1} \|\Delta \mathbf{u}[k+i]\|_{\mathbf{R}}^2 \quad (12a)$$

while being subject to:

$$\mathbf{y}[k+j+1] = \hat{\mathbf{f}}_{\mathbf{w}}(\mathbf{y}[k+j], \mathbf{u}[k+j]), \quad \forall j = 0, \dots, N_2 - 1 \quad (12b)$$

$$\mathbf{u}[k+j] = \mathbf{u}[k-1] + \sum_{i=0}^j \Delta \mathbf{u}[k+i], \quad \forall j = 0, \dots, (N_u - 1) \quad (12c)$$

$$\mathbf{u}[k+j] = \mathbf{u}[k+N_u-1], \quad \forall j = N_u, \dots, N_2 - 1 \quad (12d)$$

$$\mathbf{h}(\mathbf{y}[k+j], \mathbf{u}[k+j]) \leq 0, \quad \forall j = N_1, \dots, N_2 \quad (12e)$$

$$\mathbf{g}(\mathbf{y}[k+j], \mathbf{u}[k+j]) = 0, \quad \forall j = N_1, \dots, N_2 \quad (12f)$$

3. Experiments

3.1. Metrics

The evaluation of the PINC net prediction performance is done on a validation set in self-loop mode (Figures 3a and 4). In particular, the generalization MSE is computed only at the discrete time steps (vertical lines in Fig.4):

$$\text{MSE}_{gen} = \frac{1}{N_y} \sum_{i=1}^{N_y} \frac{1}{M} \sum_{k=1}^M (y_i[k] - \hat{y}_i[k])^2, \quad (13)$$

where: $\mathbf{y}[k]$ is the prediction of the PINC net given by equation (8) and $\hat{\mathbf{y}}[k]$ is obtained with Runge-Kutta (RK) simulation of the true model of the plant; and the same control input signal $\mathbf{u}[k]$ is given to both the PINC net and the RK model.

The control performance is measured by employing the **Integral of Absolute Error (IAE)** on a simulation of C iterations:

$$\text{IAE} = \frac{1}{N_y} \sum_{i=1}^{N_y} \frac{1}{C} \sum_{k=1}^C |r_i[k] - y_i[k]| \quad (14)$$

and the **Root Mean Squared Error (RMSE)**:

$$\text{RMSE} = \frac{1}{N_y} \sum_{i=1}^{N_y} \sqrt{\frac{1}{C} \sum_{k=1}^C (r_i[k] - y_i[k])^2} \quad (15)$$

where $r_i[k]$ is the reference value of $y_i[k]$ at timestep k .

3.2. Van der Pol Oscillator

3.2.1. Model

The Van der Pol Oscillator [28] is an ODE initially discovered by Balthazar Van der Pol that had the original purpose of modeling triode oscillations in electric circuits. Since then, the ODE has been used for other purposes, such

as seismology and biological neuron modeling [28], and as a standard proof-of-concept dynamical system for optimal control applications [29]. The equations that govern the Van der Pol Oscillator are as follows:

$$\dot{x}_1 = x_2 \quad (16a)$$

$$\dot{x}_2 = \mu(1 - x_1^2)x_2 - x_1 + u \quad (16b)$$

where $\mu = 1$ is referred to as the damping parameter, which affects how much the system will oscillate, $\mathbf{x} = (x_1, x_2)$ is the system state, and u is an exogenous control action.

By inspection, the Van der Pol oscillator has an equilibrium at $\bar{\mathbf{x}} = (u, 0)$, which is stable for a constant input $u \in (-\sqrt{3}, -1)$ or $u \in (1, \sqrt{3})$. The oscillator also has a limit cycle that can be perceived in polar coordinates [28]. For our experiments, $u \in [-1, 1]$ and $x_1, x_2 \in [-3, 3]$.

3.2.2. PINC Analysis

To find the most suitable configuration for the PINC net to control a dynamic system, we propose to first run grid search experiments over hyperparameters such as complexity of the network and number of data points (N_t) and collocation points (N_f).

Here, the sampling time is chosen as according to the problem at hand: the particular dynamics of the Van der Pol oscillator: $T = T_s = 0.5s$. At first, we use $N_t = 1,000$ and $N_f = 100,000$ as they provide a sufficient number of points to train a PINC net.

For training the PINC net, ADAM is used to optimize the loss function for $K_1 = 500$ epochs, and afterward, L-FGBS is used for $K_2 = 2,000$ iterations for enhancing the stability of the training process. Note that this K_2 does not exhaust the training, and as such, it will need to be increased before final deployment of the PINC net. The parameter λ is set empirically so that MSE_y and $MSE_{\mathcal{F}}$ are not in disparate scales. The validation dataset is composed of 1810 points obtained using a randomly generated control action u (e.g., Fig. 5), which is equivalent to 905s of simulation, since $T_s = 0.5s$. The validation or generalization error considers the self-loop mode of PINC to compute Eq. (13).

The first experiment analyses the network complexity (Fig. 6a) and shows the validation MSE using Eq. (13) averaged over 10 different random initializations of the network weights. In general, as the network grows deeper and with more neurons per layer, the performance increases. Besides, layers with 3 or 5 neurons are not enough to model the required task. Note that these errors would decrease even further if training had been extended for more epochs (*correcting* the lower performance of the net of 10 layers with 15 neurons each, for instance). Although the network of 10 layers with 20 neurons each achieves the best performance, we choose to continue the following experiments with a configuration of 4 layers of 20 neurons each, which also showed excellent performance, but with less computational overhead.

In Fig. 6b, the proportion between data points and collocation points is investigated. Each error cell in the plot corresponds to the average of 5 different

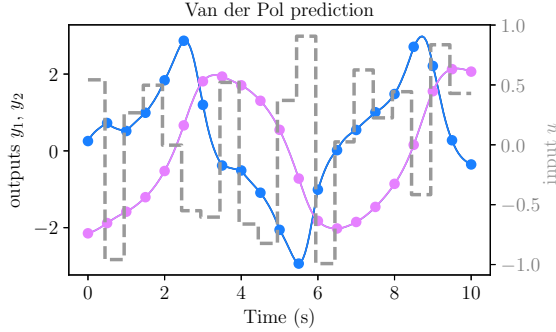


Figure 5: PINC net prediction for the Van der Pol oscillator on test data. The randomly generated input u is given by the grey dashed line, while the predictions for the oscillator states x_1 and x_2 correspond to the solid blue and pink lines, respectively. The target trajectory, from RK method, is also plot in black, but is not visible as the prediction completely superimposes the former. Each dot in the predicted trajectory corresponds to the vertical lines in Fig. 4 when control action and initial state change values (after $T_s = T = 0.5s$).

experiments with randomly generated networks. Clearly, 40 data points are not enough, and the proportion N_f/N_t should be considerably higher than 4 (hence the dark cells in the upper-right corner of the plot).

3.2.3. PINC Control

The final PINC net is chosen to have 4 hidden layers each of 20 neurons for the Van der Pol oscillator. Besides, we continue setting $N_t = 1,000$, $N_f = 100,000$, and $K_1 = 500$, but the training is extended with $K_2 = 20,000$, which allows the MSE to settle in an asymptotic curve (Fig. 7). For comparison, a vertical black dashed line is plotted in Fig. 7, indicating the moment at which training would have stopped for earlier experiments from Fig. 6. Thus, further training allows improving validation error (according to (13)) at least one order of magnitude. Note that the validation error does not increase permanently as training follows due to the regularization effect of $MSE_{\mathcal{F}}$ in the loss function.

To view the PINC prediction after training, we randomly generate a control input u for 10s. In Fig. 5, the predicted trajectory is given for such a control input. With our method, we can directly infer each circle in the trajectory using (8) every $T = 0.5s$. The trajectory between two consecutive circles can be predicted by varying the input t of the network and keeping the other inputs $y(0)$ and u fixed. The prediction matches the target trajectory very well as the latter is also plot, but gets superimposed by the former.

The resulting control from PINC can be seen in Fig. 8 in a simulation of 60s, where MPC was employed to find the optimal value of the control input, considering a prediction and control horizon of $5T$ (or $2.5s$). The control parameters are given as follows: $N_1 = 1$, $N_2 = 5$, $N_u = N_2$, $Q = 10I$ and $R = I$. Here, the optimization in MPC to find a control input at the current timestep uses the PINC network’s predicted trajectory for future timesteps, i.e., for the

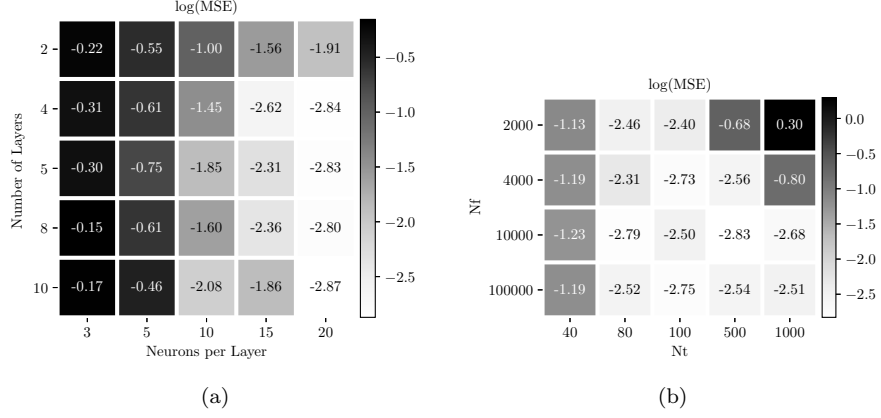


Figure 6: Analysis of the PINC net for the Van der Pol Oscillator. The network training time is fixed to a constant number of iterations. The MSE validation error is computed according to Equation (13). (a) The \log_{10} of the MSE error as a function of network complexity, averaged over 10 different simulations. The best generalization error ($10^{-2.87}$) is achieved with a deep network of 10 layers with 20 neurons each. (b) The effect of the number of collocation points N_f and data points N_t on generalization performance, averaged over 5 different randomly initialized networks.

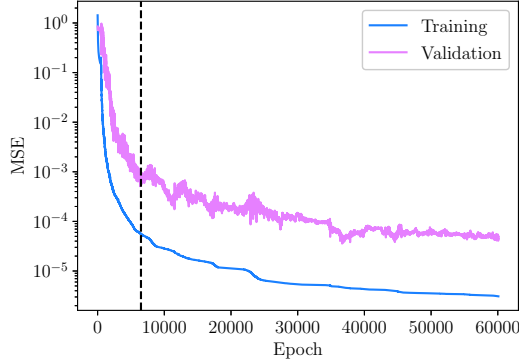


Figure 7: MSE evolution during training of the final PINC net. Previous experiments stopped training at the vertical dashed line. The validation dataset consists of 1810 points, or 90s of simulation since $T = T_s = 0.5s$. The validation MSE is more noisy because it is computed on a much smaller dataset and on self-loop mode using (13).

prediction horizon of $2.5s$. This procedure is repeated for all 120 points of the plotted trajectory. For instance, the right plot of Fig. 8 shows that five different control inputs, found sequentially by MPC, were applied to the dynamic system during the initial $2.5s$. Here, the role of the plant to be controlled is taken by the Van der Pol oscillator, whose states are obtained by an RK integrator. The control performance is presented in Table 1, which also shows the result when the original ODE model is used in MPC instead of the PINC net. In this case,

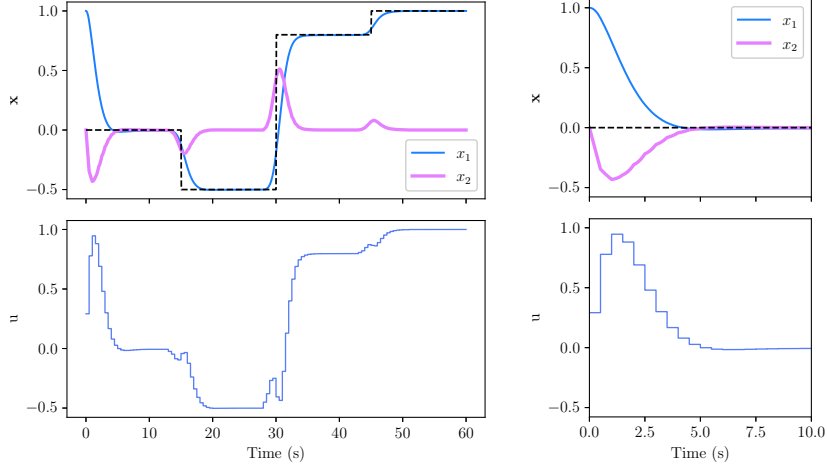


Figure 8: Control of the Van der Pol oscillator with PINC. The reference trajectory for x_1 (x_2) is given by a dashed black step signal (fixed at zero), while the controlled variables are the states x_1 and x_2 given by blue and pink lines. The control input u is the manipulated variable in the lower plot, found by MPC. Left: simulation totalling 60s. Right: close-up on the first 10s. See text for more details.

RK is employed to compute the states of the system for MPC. It is remarkable to observe that PINC achieves practically the same result of the ODE/RK approach in terms of RMSE and IAE, while being 31s slower when executed in the same desktop computer.

3.3. Four tanks

3.3.1. Model

The Four tanks system is a widely used benchmark for multivariate control systems [30], as it is a nonlinear and multivariate system with some degree of coupling between variables. By setting its parameters to a given combination of values, it is possible to induce the system to have non-minimum phase transmission zeros, which are an additional difficulty for PID controllers [30].

As Figure 9 shows, the four tanks system is composed of four tanks, denoted by the index $i = \{1, 2, 3, 4\}$, and two pumps $j = \{1, 2\}$ supplying each tank with water. Each tank has a cylindric form with a basis area of A_i , and an orifice of area a_i at the basis center. Tank 1 (2) is located right below tank 3 (4), so that the flow ω_i from the tank above goes directly to the tank below. Both pumps are linear actuators controlled by the voltage u_j with coefficient k_j converting the voltage into the pump flow. Pump 1 (2) is associated with a directional valve that distributes the resulting flow into tanks 1 and 4 (2 and 3), which is the coupling source in this system. The directional valves have an opening γ_j , which is the amount they distribute to the bottom tanks. The adjustment of γ_j is one of the main factors to regulate the control problems associated with the system [30]. The level of water in each tank is denoted h_i .

The following equations govern the four tank system, which are obtained from mass balance:

$$\dot{h}_1 = \frac{\gamma_1 k_1 u_1 + \omega_3 - \omega_1}{A_1} \quad (17a)$$

$$\dot{h}_2 = \frac{\gamma_2 k_2 u_2 + \omega_4 - \omega_2}{A_2} \quad (17b)$$

$$\dot{h}_3 = \frac{(1 - \gamma_2) k_2 u_2 - \omega_3}{A_3} \quad (17c)$$

$$\dot{h}_4 = \frac{(1 - \gamma_1) k_1 u_1 - \omega_4}{A_4} \quad (17d)$$

where the flow in each tank orifice ω_i is described by the Bernoulli orifice equation, adding the sole nonlinearity of the system:

$$\omega_i = a_i \sqrt{2gh_i} \quad (18)$$

with g as the acceleration of gravity. The parameters used for this application are the same as the ones stipulated for the non-minimum phase experiment in [30].

3.3.2. PINC Control

We have performed a similar approach to the first control problem with respect to finding a suitable configuration for network complexity and the proportion between data and collocation points. We have observed that the minimum number of layers is 5 to get enough prediction performance for the four tanks system, since it is a more complex plant, with multiple inputs and multiple outputs (MIMO) operating at different timescales. The following experiments consider a PINC net with 5 layers of 20 neurons each. Besides, we continue setting $N_t = 1,000$, $N_f = 100,000$, $K_1 = 500$, and $K_2 = 20,000$. The sampling

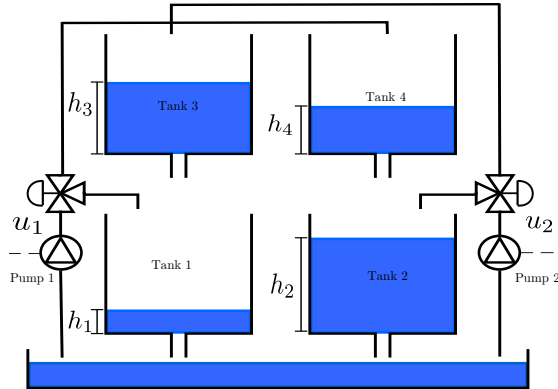


Figure 9: Schematic representation of the Four Tanks system. Figure from [23].

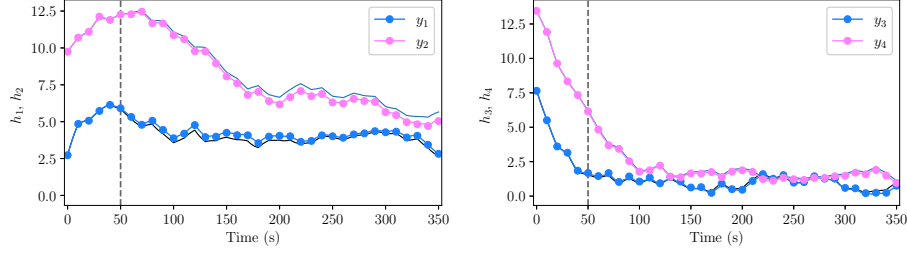


Figure 10: PINC net prediction for the four tanks system on test data, with randomly generated control input signals similar to Fig. 5. The predictions for the level of the tanks h_1 and h_2 correspond to the solid blue and pink lines, respectively. The target trajectories, from the RK method, are also plot in dark solid lines without dots. At each dot in the predicted trajectory, the PINC net receives new inputs for control action and initial state (every $T_s = T = 10s$), as explained in Fig. 3a. The vertical dashed line indicates the prediction horizon used for MPC.

period is $T = T_s = 10s$. The control parameters are once again given by $N_1 = 1$, $N_2 = 5$, $N_u = N_2$, $Q = 10\mathbf{I}$ and $R = \mathbf{I}$.

After training the PINC net, the prediction on test data, with new randomly generated control actions (not shown), is presented in Fig. 10. The deviation in prediction at longer ranges, as seen in the first plot for h_1 and h_2 , is expected, since the network works in self-loop mode, feeding its prediction of the last state back as input for the initial state (Fig. 3a), every $T = 10s$. Thus, the error is accumulated in this chaining procedure. However, MPC uses this trajectory only up to 50s, equivalent to a prediction horizon of 5 steps, indicated by the vertical dashed line in the figure, and the next optimization procedure in MPC resets the initial state to the true value as obtained by sensors of the real process (Fig. 3b).

For this four tank system, PINC's control employs prediction and control horizons both of 5 steps (50s in simulation time). Besides, both h_3 and h_4 tank levels are constrained to the interval $[0.6, 5.5]\text{cm}$. The results are shown in Fig. 11, where the controlled and constrained tank levels are presented in the first two plots, and the control action found by MPC is shown at the bottom plot. The plots on the right-hand side show a close-up during the initial 160s of simulation. The control was successful in spite of the constrains imposed on h_3 and h_4 (which were respected) and some minor error in steady regime, which can be corrected by adding the calculation of a correction factor through filtering the error between the measurement and the network prediction, as done in [31] for a recurrent network.

The control performance in terms of RMSE and IAE are shown in Table 1. Although IAE seems to differ more between PINC and ODE/RK, RMSE errors for both methods are almost equivalent. The time spent in a desktop computer for the complete control simulation in PINC, 1262s, is just relatively slightly superior to using the ODE of the four tanks as a model for MPC (1023s), which is remarkable given the architecture of 5 hidden layers with 20 neurons each

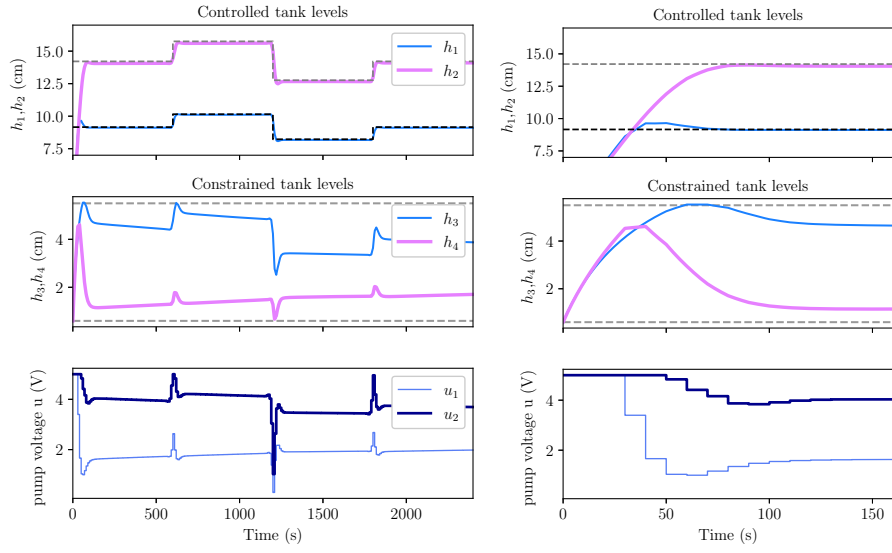


Figure 11: Control of the four tanks system with PINC. The controlled variables are the tank levels h_1 and h_2 given by blue and pink lines, respectively, whereas the reference trajectory for h_1 (h_2) is given by a dashed black (grey) step signal. The control inputs \mathbf{u} are the manipulated voltages shown in the lower plot, found by MPC. Dashed grey horizontal lines represent the lower and upper limits for both h_3 and h_4 . Left: simulation totalling 2400s. Right: close-up on the first 160s. See text for more details.

Table 1: Results for the control experiments

	Van der Pol			Four tanks		
	(4 layers of 20 units)			(5 layers of 20 units)		
	RMSE	IAE	time	RMSE	IAE	time
PINC	0.15	123.6	140s	0.811	876	1262s
ODE / RK	0.15	122	109s	0.807	544	1023s

that is used for PINC.

4. Conclusion

We have proposed a new general framework that makes physics-informed neural networks (PINNs) amenable to control methods, such as MPC, opening a wide range of application opportunities. This Physics-Informed Neural Nets-based Control (PINC) approach not only allows a PINN to work for longer-range time intervals that are not fixed beforehand without severe prediction degradation as it normally does, but also makes it easy to use such a network for MPC applications. In control applications, this framework provides a way to identify a system by integrating collected data from a plant with a priori expert knowledge in the form of ordinary differential equations. Although we only used initial conditions as real *collected* data, we expect that usage of additional data points scattered in space-time will make the training of PINC nets much faster. In future work, we intend to extend the framework to systems described by differential-algebraic equations (DAEs), and systems for which prior knowledge is uncertain (unknown parameters) as well as to apply PINC to industrial control problems, such as in oil and gas industry, for which some prior knowledge of ODEs are known in addition to very noisy data. We expect to improve the identification process in an industrial setting by using complementary sources for training deep networks (ODEs and data), making feasible a wide range of previously unsolved applications in control.

Acknowledgments

This work was funded in part by CNPq (Grant 304183/2017-2).

References

- [1] A. Tikhonov, V. Y. Arsenin, Solutions of Ill-Posed Problems, Winston and Sons, 1977.
- [2] C. M. Bishop, Pattern Recognition and Machine Learning (Information Science and Statistics), Springer, 2006.

- [3] N. Srivastava, G. Hinton, A. Krizhevsky, I. Sutskever, R. Salakhutdinov, [Dropout: A simple way to prevent neural networks from overfitting](#), Journal of Machine Learning Research 15 (56) (2014) 1929–1958.
URL <http://jmlr.org/papers/v15/srivastava14a.html>
- [4] M. Raissi, P. Perdikaris, G. E. Karniadakis, Physics informed deep learning (Part I): Data-driven solutions of nonlinear partial differential equations, arXiv preprint arXiv:1711.10561.
- [5] M. Raissi, P. Perdikaris, G. E. Karniadakis, Physics-informed neural networks: A deep learning framework for solving forward and inverse problems involving nonlinear partial differential equations, Journal of Computational Physics 378 (2019) 686–707. doi:0.1016/j.jcp.2018.10.045.
- [6] Y. Zhu, N. Zabaras, P.-S. Koutsourelakis, P. Perdikaris, Physics-constrained deep learning for high-dimensional surrogate modeling and uncertainty quantification without labeled data, Journal of Computational Physics 394 (2019) 56–81. doi:10.1016/j.jcp.2019.05.024.
- [7] J. Sirignano, K. Spiliopoulos, DGM: A deep learning algorithm for solving partial differential equations, Journal of Computational Physics 375 (2018) 1339–1364. doi:10.1016/j.jcp.2018.08.029.
- [8] M. Raissi, Forward-backward stochastic neural networks: Deep learning of high-dimensional partial differential equations, arXiv preprint arXiv:1804.07010.
- [9] X. Meng, Z. Li, D. Zhang, G. E. Karniadakis, PPINN: Parareal physics-informed neural network for time-dependent PDEs, Computer Methods in Applied Mechanics and Engineering 370 (2020) 113250. doi:10.1016/j.cma.2020.113250.
- [10] P. Stinis, [Enforcing constraints for time series prediction in supervised, unsupervised and reinforcement learning](#), in: Proceedings of the AAAI 2020 Spring Symposium on Combining Artificial Intelligence and Machine Learning with Physical Sciences, Vol. 2587, 2020.
URL http://ceur-ws.org/Vol-2587/article_5.pdf
- [11] L. Yang, X. Meng, G. E. Karniadakis, B-PINNS: Bayesian physics-informed neural networks for forward and inverse PDE problems with noisy data, arXiv preprint arXiv:2003.06097.
- [12] G. Pang, G. E. Karniadakis, Physics-informed learning machines for partial differential equations: Gaussian processes versus neural networks, Kevrekidis P., Cuevas-Maraver J., Saxena A. (eds) Emerging Frontiers in Nonlinear Science. Nonlinear Systems and Complexity 32 (2020) 323–343.
- [13] L. T. Biegler, Nonlinear Programming: Concepts, Algorithms, and Applications to Chemical Processes, SIAM, Philadelphia, 2010.

- [14] L. Grüne, J. Pannek, *Nonlinear Model Predictive Control: Theory and Algorithms*, Springer, 2011.
- [15] E. F. Camacho, C. Bordons, *Model Predictive Control*, Springer Science & Business Media, 2013.
- [16] J. P. Jordanou, E. Camponogara, E. A. Antonelo, M. A. S. Aguiar, Nonlinear model predictive control of an oil well with echo state networks, *IFAC-PapersOnLine* 51 (8) (2018) 13–18. doi:[10.1016/j.ifacol.2018.06.348](https://doi.org/10.1016/j.ifacol.2018.06.348).
- [17] U. Eren, A. Prach, B. B. Koçer, S. V. Raković, E. Kayacan, B. Açıkmeşe, Model predictive control in aerospace systems: Current state and opportunities, *Journal of Guidance, Control, and Dynamics* 40 (7) (2017) 1541–1566. doi:[10.2514/1.G002507](https://doi.org/10.2514/1.G002507).
- [18] T. P. Nascimento, C. E. T. Dórea, L. M. G. Gonçalves, Nonlinear model predictive control for trajectory tracking of nonholonomic mobile robots: A modified approach, *International Journal of Advanced Robotic Systems* 15 (1). doi:[10.1177/1729881418760461](https://doi.org/10.1177/1729881418760461).
- [19] J. P. Jordanou, E. A. Antonelo, E. Camponogara, Echo state networks for practical nonlinear model predictive control of unknown dynamic systems, Submitted for publication.
- [20] D. P. Kingma, J. Ba, ADAM: A method for stochastic optimization, arXiv preprint arXiv:1412.6980.
- [21] G. Andrew, J. Gao, Scalable training of L1-regularized log-linear models, in: *Proceedings of the 24th International Conference on Machine Learning, ICML'07*, Association for Computing Machinery, New York, NY, USA, 2007, pp. 33–40. doi:[10.1145/1273496.1273501](https://doi.org/10.1145/1273496.1273501).
- [22] J. E. Normey-Rico, E. F. Camacho, *Control of Dead-time Processes*, Springer London, 2007. doi:[10.1007/978-1-84628-829-6](https://doi.org/10.1007/978-1-84628-829-6).
- [23] A. S. M. Brandão, *Controle preditivo com geração de código: Um estudo comparativo*, Master's thesis, Universidade Federal de Santa Catarina (2018).
- [24] J. Nocedal, S. J. Wright, *Numerical Optimization*, 2nd Edition, Springer, New York, NY, USA, 2006.
- [25] P. E. Gill, W. Murray, M. A. Saunders, SNOPT: An SQP algorithm for large-scale constrained optimization, *SIAM Review* 47 (2005) 99–131. doi:[10.1137/S0036144504446096](https://doi.org/10.1137/S0036144504446096).
- [26] A. Wächter, L. T. Biegler, On the implementation of an interior-point filter line-search algorithm for large-scale nonlinear programming, *Mathematical Programming* 106 (1) (2006) 25–57. doi:[10.1007/s10107-004-0559-y](https://doi.org/10.1007/s10107-004-0559-y).

- [27] A. Iserles, A First Course in the Numerical Analysis of Differential Equations, Cambridge University Press, 1996.
- [28] H. Y. Hafeez, C. E. Ndikilar, S. Isyaku, Analytical study of the Van der Pol equation in the autonomous regime, Progress in Physics 11 (2015) 252–255.
- [29] J. Andersson, J. Åkesson, M. Diehl, Dynamic optimization with CasADi, in: Proceedings of the IEEE Conference on Decision and Control, 2012, pp. 681–686. [doi:10.1109/CDC.2012.6426534](https://doi.org/10.1109/CDC.2012.6426534).
- [30] K. Johansson, The quadruple-tank process: A multivariable laboratory process with an adjustable zero, IEEE Transactions on Control Systems Technology 8 (2000) 456–465. [doi:10.1109/87.845876](https://doi.org/10.1109/87.845876).
- [31] J. P. Jordanou, E. Camponogara, E. A. Antonelo, M. A. S. Aguiar, Nonlinear model predictive control of an oil well with echo state networks, IFAC-PapersOnLine 51 (8) (2018) 13–18. [doi:10.1016/j.ifacol.2018.06.348](https://doi.org/10.1016/j.ifacol.2018.06.348).